

Diagnosing cyclogenesis by partitioning energy and potential enstrophy in a linear quasi-geostrophic model

By DANIEL HODYSS* and RICHARD GROTJAHN, *Atmospheric Science Program, Department of Land, Air, and Water Resources, University of California, Davis, CA 95616, USA*

(Manuscript received 8 June 2000; in final form 6 April 2001)

ABSTRACT

Baroclinic development is studied with 2 linear, quasi-geostrophic models. One model is the Eady model, the other uses more realistic wind, density, Coriolis, and static stability. Initial-value solutions are diagnosed using time series of potential enstrophy (H), total energy (E), the components of H and E , and the amplitude norm. Two vertical structures for the initial condition are used for both models. One initial condition is representative of a class of initial conditions studied previously having enhanced nonmodal growth (NG). The other initial condition approximates observed conditions prior to cyclogenesis. Results are shown for the most unstable normal mode wavelength of each model. The growth rates of the components of H and E evolve quite differently for different initial states and models tested. NG in H is shown to be sensitive to the contribution of the boundary potential vorticity (BPV) of the initial state; small adjustments in eddy structure at the boundary significantly alter BPV and H growth rates. The amount of NG is related to how far BPV present initially differs from the asymptotic normal mode. The effect upon NG of each approximation present in the Eady model (but not in the other model) are considered. Using realistic mean flow shear, static stability, or compressibility can significantly reduce NG but including linearly varying Coriolis parameter did not. Two conceptual models of NG are considered. Growth by increasingly favorable superposition remains relevant. Growth by “tilting into the vertical” is shown to be incorrect.

1. Introduction

Studies into the mechanisms of baroclinic instability often focus upon two growth mechanisms: unstable normal modes and “nonmodal” growth (NG). Charney (1947) and Eady (1949) examine the growth of perturbations on basic states with vertical shear only. They found unstable “normal mode” eigenfunctions for the linearized, quasi-geostrophic (QG) equations that grow exponentially. When the equations are solved as initial value problems using more general initial eddy structures, the eddy can change shape and can have temporary amplification. When this

amplification exceeds the unstable normal mode growth rate, it shall be referred to as “nonmodal growth” (NG) here.

This study reports on initial-value calculations using two linear QG models and two distinct initial conditions (ICs). Both ICs are used in an earlier report in *Tellus* (Grotjahn and Tribbia, 1995). One IC (Fig. 1a) consists of troughs and ridges that each have upstream tilt and are each continuous throughout the troposphere; if a stratosphere is present in the model, this mode decays exponentially above the tropopause without further upstream tilt. Following the naming used by Grotjahn and Tribbia, this IC will be labelled the “connected” case. Similar ICs have been used by Farrell (1984, 1985), Grotjahn et al. (1995b), and others. In Grotjahn et al. (1995b) it was shown

* Corresponding author.
e-mail: dhodyss@ucdavis.edu

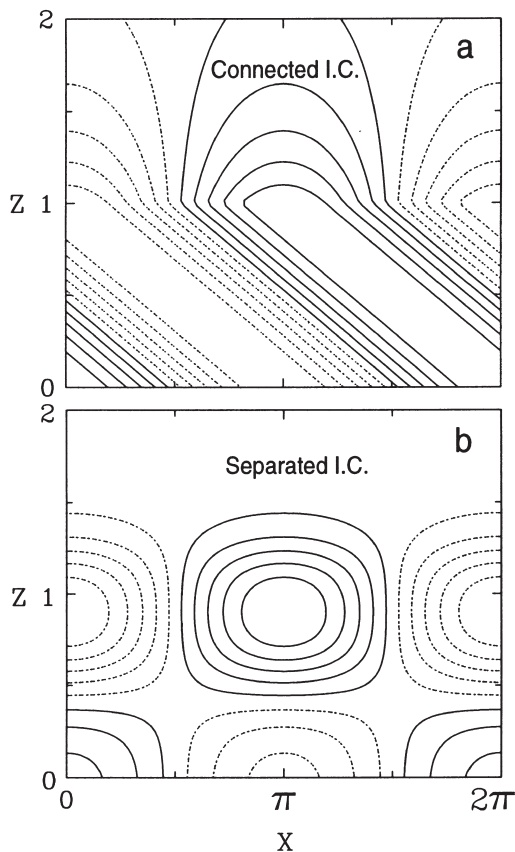


Fig. 1. Height versus longitude plots of stream function for the two primary initial conditions (ICs) used in this study. Negative-valued contours of stream function are dashed. (a) connected IC, (b) separated IC. The abscissa is in radians while the ordinate is nondimensional height. The Eady model only extends to $z = 1.0$

that the amount of upstream tilt had little effect upon the magnitude of the peak growth rate, but did alter the timing: peak growth occurred later for larger upstream tilt. Hence, results for this IC can represent a wider class of initial conditions having upstream tilt and similar amplitude throughout the troposphere.

The other IC is an archetype for observed conditions prior to cyclogenesis. Prior to development (Grotjahn, 1996) observed troughs are not connected and each has little or no upstream tilt. This IC consists of separate, upper and lower troughs (and ridges) in the troposphere. Each trough and ridge initially has no vertical tilt.

Fig. 1b shows the structure of this “separated” case IC. The results for this IC have broader applicability. Varying the relative magnitudes of the upper and lower features by a factor of two changes the details but not the general conclusions drawn here.

The amount of NG and the evolution through time to reach the most unstable normal mode structure was shown by Grotjahn and Tribbia (1995) to be substantially different between these two ICs. This study is motivated in part to understand better why the NG should be so different. A second motivation is to examine why the growth is also different between the two models. Finally, the NG that develops varies between the parameters tracked over time. For example, amplitude may have notable NG while energy does not in a given calculation. Better understanding of how and why these differences arise helps to clarify the nonmodal mechanism and the instability problem.

The issue of nonmodal development is usually shown in the growth rate of various integral quantities. Growth rate of total energy (E) has been included in studies by: Farrell (1982), Grotjahn et al. (1995b), Rotunno and Bao, 1996; Dong and James (1997). Some studies have examined growth rates of streamfunction or geopotential amplitude (Grotjahn, et al., 1995b; Grotjahn and Tribbia, 1995; Rotunno and Bao, 1996). Growth rates of QG potential enstrophy (H) have also been tracked over time (Grotjahn, et al., 1995b; Grotjahn and Tribbia, 1995). Other studies have examined the structures that maximize the growth of E , H , and/or amplitude at a moment or over a finite time (O’Brien, 1992; Joly, 1995). Few studies further partition the integral quantity by examining growth rates of the components (Dong and James, 1997). (To be fair, additional studies show time series of the components, but it is generally impractical to discern growth rates from such figures.) However, Joly (1995) shows peak growth rates of singular vectors for kinetic and available potential components of E . Fischer (1998) considers enstrophy and potential energy growth optimized over finite times in the Eady model. We have not identified any report tracking the growth rates of the components of H and E and this paper is intended to fill that gap. The utility of partitioning H and E is illustrated here primarily using a model described in Grotjahn (1980) and hereafter labeled the G model. The G

model removes several major assumptions present in the Eady model. A further motivation arises because the NG and its partition amongst the components of H and E differs in the G model from the commonly-used Eady model.

In Section 2, the numerical model and the diagnostic quantities used to evaluate the solution through time are described. Section 3 applies the diagnostic procedure to the Eady and G models. Conclusions are summarized in Section 4.

2. Model description and diagnostics

2.1. Model description

The linearized quasi-geostrophic potential vorticity (QGPV) equation and its usual boundary conditions in the vertical are:

$$\left(\frac{\partial}{\partial t} + U \frac{\partial}{\partial x}\right) \times \left[\nabla^2 \Psi + \frac{1}{\rho} \frac{\partial}{\partial z} \left(\rho \varepsilon \frac{\partial \Psi}{\partial z} \right) \right] + \frac{\partial Q}{\partial y} \frac{\partial \Psi}{\partial x} = 0, \quad (1a)$$

$$\left(\frac{\partial}{\partial t} + U \frac{\partial}{\partial x}\right) \left(\frac{\partial \Psi}{\partial z} \right) - \frac{\partial U}{\partial z} \frac{\partial \Psi}{\partial x} = 0 \quad \text{at } z=0, z^{\text{top}}, \quad (1b)$$

where Ψ is the perturbation streamfunction,

$U = U(z)$ is the prescribed basic state zonal wind,

$$\frac{\partial Q}{\partial y} = \beta - \frac{1}{\rho} \frac{\partial}{\partial z} \left(\rho \varepsilon \frac{\partial U}{\partial z} \right)$$

is the meridional gradient of the basic state potential vorticity, $\rho = \rho(z)$ is the basic state density and $\varepsilon = (f_0 L / ND)^2$. N is the Brunt Väisälä frequency and ε is the squared ratio of the assumed length scale (L) over the Rossby radius of deformation. Other parameters are: constant Coriolis parameter f_0 , vertical length scale D , constant $\beta = df/dy$, where f is the linearly varying Coriolis parameter. In the Eady model density and static stability are constants. In the G model vertical profiles of density and static stability are chosen to match the US Standard Atmosphere (1976) (see Grotjahn (1980) for a complete description). The prescribed zonal wind increases linearly with height in the Eady model. In the G model, the prescribed zonal wind reaches a maximum at the simulated tropopause ($z = 1.0$) and decreases into the stratosphere. Fig. 2 shows these prescribed parameters.

The models are linear and nondimensional; they use Cartesian coordinates. The G model uses a mid-latitude beta plane (linear Coriolis parameter). The equations have been made nondimensional using typical scaling magnitudes for: horizontal length ($L = 1000$ km), vertical depth

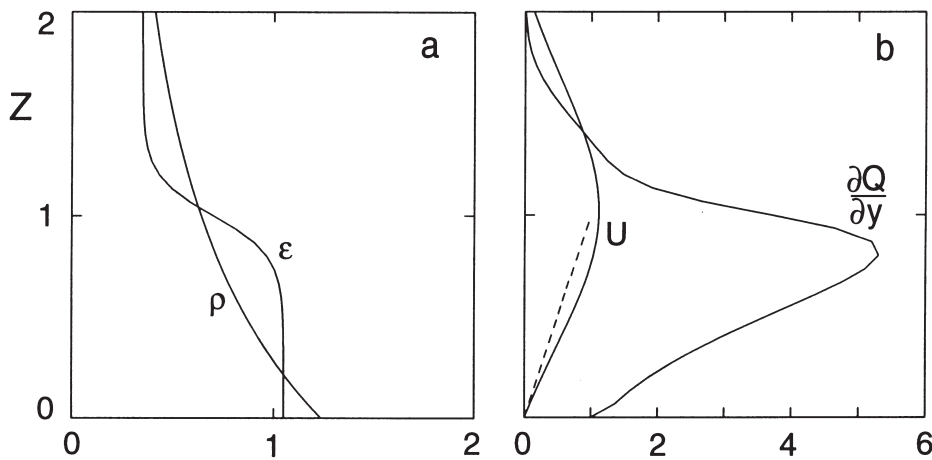


Fig. 2. Vertical profiles of basic state properties in the G (solid lines) and Eady (dashed line) models. Density (ρ) and ε are both 1.0 in the Eady model. Interior $\partial Q / \partial y = 0$ in the Eady model. Basic state meridional gradient of Q at the surface (including BPV contribution) using 31 levels is -39 for the G model and -59 for the Eady model.

($D = 10$ km), speed ($V = 10 \text{ ms}^{-1}$), and the advective time scale ($L/V = 10^5$ s).

This set of equations is solved numerically as an initial-value problem. The numerical model is spectral in the horizontal, uses second-order finite differences in the vertical and the 3rd order Adams–Bashforth scheme is used for integration through time. The model uses 31 levels in the vertical. The model is fully three dimensional, but the experiments shown here use a very large meridional wavelength. The results shown use the zonal wavelength, k , of the most unstable normal mode. The most unstable wavenumber is $k = 1.6$ for the Eady model and $k = 2.05$ for the G model.

2.2. Diagnostics

The growth in the solution is measured by calculating various dynamical properties of the disturbance. The most common properties are the mass-weighted, volume integrals of total energy (E), potential enstrophy (H), and root mean square perturbation amplitude (L2 norm). The integrals in these quantities are solved numerically using the Simpson 1/3 rule.

The exponential growth rate of a quantity F is given by

$$\sigma_F = \frac{1}{F} \frac{dF}{dt}. \quad (2)$$

This rate asymptotes to twice the growth rate of the most unstable normal mode if F is E or H since those are squared quantities; σ_F asymptotes to the normal mode growth rate if F is the L2 norm.

The integrated mass weighted total energy is defined as

$$E = \frac{1}{2} \int_V \rho (\Psi_x^2 + \Psi_y^2 + \varepsilon \Psi_z^2) dv, \quad (3)$$

where subscripts denote differentiation. The first two terms comprising the integrand are the kinetic energy (KE) and the last term represents the available potential energy (APE). The KE and APE terms shall be evaluated separately, as well as summed ($= E$).

The Eady and G models only allow baroclinic energy conversions. Hence,

$$\frac{dE}{dt} = \int_V \rho \varepsilon U_z \Psi_x \Psi_z dv. \quad (4)$$

If the basic state wind (U) increases with height, then a positive correlation between the eddy meridional wind (Ψ_x) and the eddy potential temperature (Ψ_z) will increase the perturbation energy.

Another measure of growth during the evolution of a cyclone is the potential enstrophy integral:

$$H = \frac{1}{2} \int_V \rho q^2 dv, \quad (5)$$

where q is the perturbation QGPV in the model's numerical form of interior and boundary potential vorticity. The continuous differential expression for the components of q^* is (Bretherton, 1966; Lindzen and Tung, 1978):

$$q^* = \nabla^2 \Psi + \frac{1}{\rho} \frac{\partial}{\partial z} \left(\rho \varepsilon \frac{\partial \Psi}{\partial z} \right) + \varepsilon \left(\frac{\partial \Psi}{\partial z} \delta(z) - \frac{\partial \Psi}{\partial z} \delta(z - z^{\text{top}}) \right). \quad (6)$$

O'Brien (1992) has shown that q^* in (6) is numerically equivalent to the QGPV obtained from (1) in the limit of vanishing grid interval. We obtain the total q at the boundaries prior to squaring when evaluating (5). An alternative procedure has been suggested (Hakim, 2000) where the two boundary PV terms are separately squared and added to the integrated interior PV squared. The first term in (6) is the relative vorticity (RV), the second term is labeled "thermal" vorticity (TV), and the third term is the potential vorticity due to a potential temperature gradient on the top and bottom boundaries (BPV). When only RV is used in (5) it is labeled the RV^2 integral. Similarly, TV^2 and BPV^2 integrals are defined using just TV and just BPV in (5). In order to facilitate comparison with the growth rate of H , it is useful to examine what may change H .

The potential enstrophy varies in time according to

$$\frac{dH}{dt} = - \int_V \rho \Psi_x q Q_y dv. \quad (7)$$

(see, e.g., Grotjahn (1993), p. 369, 7.4 for a review). For a positive meridional gradient in basic-state QGPV ($Q_y > 0$), a negative correlation between the eddy meridional wind (Ψ_x) and the eddy QGPV (q) increases the perturbation potential enstrophy. "Star" superscripts are not used in (7) because numerical model expressions are used in practice when evaluating q and Q_y . In the Eady

model $Q_y = 0$ in the interior and exists only at the boundaries, so that time changes in H can only occur from correlations on the boundaries. The more general G model has nonzero interior Q_y , but the boundary Q_y is still much larger and growth in potential enstrophy remains largely forced by the boundaries. Examination of the eigenmodes for the G model shows large surface BPV in the normal modes, but minimal BPV in *most* but not all of the continuum modes. This property contrasts with the Eady model where all normal and continuum modes have at least a moderate amount of BPV.

From (7), one may deduce the contributions to H by looking at the respective meridional fluxes of RV, TV and BPV. When that is done, the growth rate time series is dominated by the BPV flux. The TV flux is much less: it is consistently about one tenth of the total in the G model. The integrated RV flux contribution to the potential enstrophy growth rate is zero. This pattern holds for both cases and both models and so need not be shown. Instead, growth rate time series for TV^2 , RV^2 , and BPV^2 integrals are discussed since there is interesting variation of these quantities.

NG can be viewed as superposition of overlapping modal properties (Rotunno and Fantini, 1989; Davies and Bishop, 1994; Grotjahn et al., 1995b; and others). A general initial condition (such as those used here) has interior and boundary perturbation q . The q projects onto the complete spectrum of eigenmodes. Consulting (7) these modes propagate and their q components are advected at different rates. The total H may amplify from eddy PV fluxes at the boundary and, for the G model, interior fluxes too. In the Eady model there is more overlap of eigenmodes' boundary q than in the G model. But, the q of the eigenmodes has much greater overlap in the interior (see Grotjahn et al., 1995a) of the G model. ("Continuum" eigenmodes in the Eady model have non-zero q at the critical level.) Sorting out the superposition for a general initial condition is possible by examining the modes present (based on their projections) but a simpler way to sort out the NG *in the aggregate* is to examine the components of q .

Another view is that NG arises from reduction of upstream tilt. The tilt of the total solution can be linked to increasingly favorable superposition. Neutral modes (be they normal modes or con-

tinuum modes) have no tilt. Furthermore, neutral modes with mainly upper level amplitude move faster than lower level modes (when the basic wind increases with elevation). Hence, the superposition increases as the total solution changes tilt from upstream to becoming more vertical, i.e., the modes are becoming more favorably aligned. This change of tilt also implies changes in the components of q ; thus NG is sometimes described as TV (and possibly BPV) being converted into RV. If RV is growing then so is the perturbation amplitude (Fischer, 1998).

Amplitude growth is commonly revealed using this norm:

$$L2 = \left(\int_V \rho \Psi^2 dv \right)^{1/2}. \quad (8)$$

3. Solutions

3.1. Overview

Solutions for the connected and separated initial conditions (Fig. 1) are presented with emphasis upon the G model results. Analogous simulations with the Eady model are noted for comparison with past works. The G model has no short wave cut-off. Representative solutions are shown for the most unstable normal mode, near $k = 2$ for the G model (and near $k = 1.6$ for the Eady model).

Before discussing growth rates results, it is useful to define an "excess growth" (EG) ratio. The EG ratio is the peak growth rate divided by the asymptotic value (due to the most unstable normal mode present). When this ratio exceeds 1.0 then NG is clearly present. Nonmodal growth may occur even when the instantaneous growth rates are less than the most unstable mode growth rate; for example, when the unstable mode is a small fraction of the total solution. However, this ratio is a simple parameter that facilitates comparison between the strength of the nonmodal mechanism for different properties of a given initial condition.

Table 1 summarizes key properties of the growth rates of H and E as well as their components. Peak values as well as asymptotic values are shown; the latter correspond to the most unstable normal mode. The table indicates that growth rates in excess of the normal mode growth rate occur sooner for the connected than for the separate initial conditions. For the energy integral (3)

Table 1. Normalized peak growth rates of various integral quantities at the wavenumber (k) of the most unstable normal mode. EG means normalization by the asymptotic value; nondimensional time, scaled by 10^5 s, of peak growth rate indicated; simulations shown for two initial states in two models

Growth rate	Eady model ($k = 1.6$) normal mode growth rate: 0.31		G model ($k = 2.05$) normal mode growth rate: 0.44	
	connected EG, time	separated EG, time	connected EG, time	separated EG, time
σ_H	1.58, 0.77	2.10, 0.88	1.25, 0.92	1.25, 2.0
σ_E	1.32, 0.51	1.16, 2.7	1.25, 0.085	1.00, 7.6
σ_{L2}	1.60, 0.0	1.24, 2.5	1.64, 0.0	1.01, 7.9
σ_{TV}	1.26, 3.23	0.95, 10.0	1.07, 3.1	1.00, 4.0
σ_{BPV}	1.77, 0.48	3.87, 0.44	1.70, 0.01	3.52, 0.34
$\sigma_{RV} = \sigma_{KE}$	1.60, 0.0	1.24, 2.5	1.64, 0.0	1.01, 7.9
σ_{APE}	1.26, 0.69	1.13, 2.7	1.04, 0.28	1.01, 5.6

and L2 norm, NG is greater for the connected case, as reported before. However, the potential enstrophy integral (5) has greater NG for the separated IC, a result that may be surprising since E , TV , APE , $L2$ (and thus RV and KE) all have less NG for this IC.

3.2. Potential enstrophy components

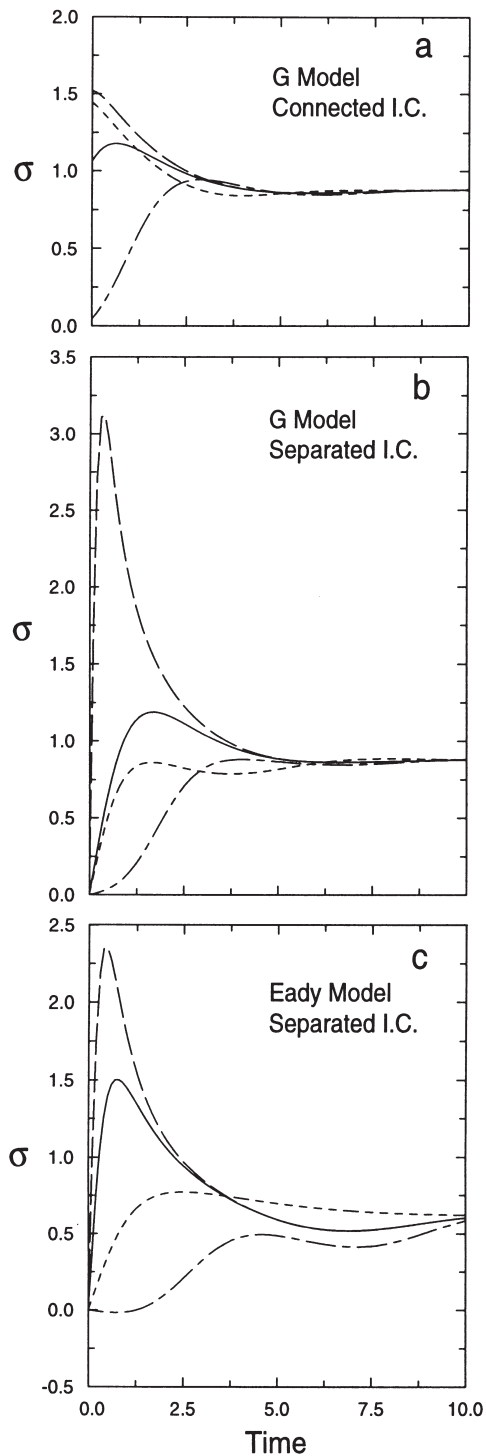
The bulk of the growth rate of H is due to meridional fluxes of BPV . Table 1 and Fig. 3 show that BPV^2 also has large NG especially for the separated IC thus causing H to have larger NG for the separated IC. Both initial conditions have distributions of the components of q^* that differ greatly from the unstable mode. Table 2 implies that TV^2 is much larger than either RV^2 or BPV^2 and that BPV^2 is nearly negligible for the separated IC. The amount of BPV at the start seems to play a crucial rôle in the amount of NG that develops in the H growth rates. This conclusion is supported by testing variations on the separated IC.

The separated IC used here has very small BPV . This IC has a maximum value but small vertical derivative (in stream function) at the bottom boundary. Hence, the initial state has very little surface temperature gradient and thus very little BPV . The BPV^2 integral growth rate includes the BPV in the denominator, so this integral develops large NG at the start as it adjusts. At the same time, the fraction of TV present in the IC is much larger than for the growing normal mode and since TV^2 grows very slowly, NG in H

is much less than the NG in BPV^2 . This point is reinforced by three variations on the separated initial condition.

The first variation on the separated IC replaces the values at the two lowest grid points (below $z = 0.1$ units) with a linear extrapolation using the slope at $z = 0.1$; initial root mean square (RMS) BPV is 2.5 times larger after this modification. This “linear” IC is difficult to distinguish from the original when plotted, but the NG both in the BPV^2 integral and in H are dramatically reduced by this modification (Table 3). A second modified separated IC sets the bottom grid point equal to the next interior grid point. The change makes BPV zero initially. This “no BPV ” IC has largest EG ratio of H . A third variation on the separated IC uses the two eigenmodes having the largest projection onto the separated IC: those are the growing and decaying normal modes. (The largest projection onto any continuum mode is more than 5 times smaller.) There is more BPV present in this “two-mode” IC than for the separated IC because each of the two modes has large BPV and the modes are offset at the bottom. The growth rate never exceeds the asymptotic value. Hence, NG in H can be strong when there is initially little BPV (relative to the most unstable normal mode); NG is less when the BPV fraction of H differs less from the normal mode fraction.

Consulting the components also helps explain results that do not conform to the “tilting into the vertical” conceptual model of NG as described above. An example is the evolution of an initial state with neither vertical tilt nor vertical variation.



This "vertical" IC is similar to the connected trough (Fig. 1a) except the axes are vertical, not tilted. Analytic solutions for this IC in the Eady model can be found in Farrell (1984) and in Simmons and Hoskins (1979). In Grotjahn et al. (1995b) the $L2$ norm starts with negative growth rate for this IC; the "tilting" conceptual model predicts this if APE is growing at the expense of KE (and hence RV). Initially, TV and BPV are zero so that H is entirely RV squared. However, H not only has positive growth rate but $EG > 1$ in this case. The reason is because early on both TV^2 and BPV^2 have very large growth rates: $EG > 2$ for $t < 1.0$. Interestingly, BPV and TV are developing in tandem, maintaining a ratio of RMS values very close to the normal mode ratio from the earliest time steps. H has peak EG ratio of 3 at $t = 0.4$ but RV still dominates the other parts of q^* . RMS RV versus RMS TV is 25 times the normal mode fraction at $t = 0.4$. The RV^2 growth rate is less than the normal mode rate until about time 3, consistent with the emergence of the unstable normal mode. The Eady model has similar time series except that the EG ratio of H is much larger than in the G model. The challenge is to explain how H can have such large NG when the largest component (by far) is growing at a rate well below the normal mode value.

From the information above, one expects the answer to flow from examination of BPV since meridional fluxes of BPV dominate the growth rate of H . Even though BPV is initially small, a flux quickly develops and continues to grow rapidly since BPV has large NG as well. One might expect the axes in the vertical IC to tilt downstream with height, but instead, upstream tilt (against the basic state shear) forms immediately. Furthermore, the amplitude profile quickly approximates a normal mode. Top and bottom maxima are easily seen in zonal cross sections by

Fig. 3. Growth rates of H (solid line) and selected components: RV^2 (short dashed line), TV^2 (dot-dashed line), and BPV^2 (long dashed line). H is quasi-geostrophic potential enstrophy, RV is relative vorticity, TV is "thermal" vorticity, and BPV is the potential vorticity from a temperature gradient at the top and bottom boundaries. See text for definitions. Shown are G model results using (a) connected and (b) separated IC and (c) the Eady model using the separated IC. Abscissa is non-dimensional time.

Table 2. RMS potential enstrophy components and energy in the two main initial conditions and for the most unstable normal mode (asymptotic value) at wavenumber (k)

	Eady model ($k = 1.6$)			G model ($k = 2.05$)		
	connected initial	separate initial	asymptotic	connected initial	separate initial	asymptotic
$ RV / TV $	0.26	0.21	0.99	0.29	0.39	0.62
$ BPV / TV $	0.32	0.08	0.99	0.25	0.06	0.64
KE/APE	0.26	0.30	0.58	0.48	0.47	0.89

Table 3. G model EG ratios for variations on the separated IC

	BPV	H
original	3.6	1.24
linear	1.5	1.1
no BPV	∞	1.39
2-mode	≤ 1	≤ 1

$t = 1.0$. The solution evolves similarly in the Eady and G models. The vertical IC has largest projection onto the two normal modes in both models. In the G model, the continuum modes with largest projections onto this IC also have structures, near the tropopause or near the bottom, rather like the normal modes. Continuum modes that have mainly mid-tropospheric maxima have comparatively small projection. (The Eady and G model continuum mode structures differ significantly and are discussed in Grotjahn et al. (1995a).) For the Eady model normal mode, RV and TV sum to zero and only the BPV portion of q^* contributes to H growth. In the G model, RV and TV still have some cancellation so they are still a smaller fraction of q than is BPV. When the solution begins to look similar to a normal mode, TV and RV largely cancel and the BPV growth rate starts to dominate the growth rate of H . Since the total solution looks like a normal mode while BPV still has large NG, then H has large NG too. These results suggest that the “tilting” viewpoint is not comprehensive as a metaphor for NG; tilt against the vertical shear is developing in this case and yet NG is large.

The superposition metaphor does explain the NG in H . The vertical derivatives are zero in the vertical IC so BPV is zero. Projecting the eigenmodes onto this vertical IC finds large amplitude BPV in the 2 normal modes that is exactly can-

celed by the BPV of the sum of the continuous spectrum. At the bottom, the normal mode BPV aggregate moves faster than the continuous spectrum BPV aggregate. BPV is “uncovered” as the relative phase between the modes has less cancellation and that leads to large NG.

The Eady model simulations for the connected (not shown) and separated ICs are generally similar to the G model results. Fig. 3c shows growth rates of H and its components for the separated IC. The main exceptions are these. First, the asymptotic (normal mode) growth rate is much less (Table 1) so it takes about twice as long for the normal mode to emerge. Second, the amount of NG present is generally larger particularly for the separated IC. The EG ratio for BPV² is similar between the two models. The RV² integral growth rates have similar EG ratio for the connected IC, though NG is stronger for the separated IC in the Eady model. The larger NG in the Eady model occurs mainly because of larger NG in TV². Third, the growth rate time series of TV² for the connected IC (not shown) is *negative* in the Eady model during the first unit of time (it is positive throughout the G model integration). Eventually, TV² recovers to exceed the normal mode value (Table 1). TV² has greater “roller coaster” oscillations at the start (Fig. 3c).

The G model improves upon the Eady model several ways and generally has less NG. The effects on NG of these improvements were tested by modifying and running the Eady model with just one G model improvement at a time. The separated IC was chosen since it shows stronger differences between the models. Compressibility and realistic static stability have negligible effect upon the normal mode growth rate at $k = 1.6$ consistent with Green (1960) and Grotjahn (1980). Compressibility and static stability modifications

have little effect upon growth rates of RV^2 and BPV^2 , but TV^2 is reduced at early times ($t < 2.5$) even becoming more negative. Since TV is the largest fraction of q^* in the IC, H is reduced as well. The realistic static stability lowers the EG ratio of H by about 10%. The zonal wind in the G model has larger vertical shear in the lower two thirds of the troposphere, but much less above in order for the wind to reach a maximum near tropopause level. The higher shear makes the modified Eady normal mode growth rate at $k = 1.6$ about 30% larger. As a result, RV^2 , BPV^2 , and H have dramatically smaller EG ratios; for H the ratio is about 40% smaller. The asymptotic values are reached sooner, too.

Ironically, TV^2 grows more quickly and now exceeds the normal mode growth rate slightly (near $t = 4.8$). Introducing linearly-varying Coriolis parameter causes the normal mode growth rates to decline by about 15% at $k = 1.6$. The initial oscillations take longer. Peak values of H and BPV^2 are similar to the standard Eady model, but since the normal mode growth rate declined, the EG ratios are higher by about 25%. The “roller coaster” variation in TV growth rate is even more pronounced. In short, most of the improvements to the Eady model reduce the NG present in H .

3.3. Energy components

The connected IC has troughs and ridge axes that tilt (upstream) against the mean flow shear. Therefore, this IC has: temperature displaced from the mass field, zonal mean meridional eddy heat fluxes, and large initial growth in the total energy as expected from (4). In the separated IC the amplitude does change with height but there is no upstream tilt, and so the heat fluxes are small in a volume average. Consequently, E grows much more slowly at the start and has little or no NG for the separated IC.

Figs. 4a,b show the time series of growth rates for E , KE , and APE for the G model. Again, connected and separated ICs are plotted. Examining the components reveals that the bulk of the NG in the connected case is due to rapid KE growth (Table 1). The peak APE growth rates are only slightly greater than the normal mode value. Fig. 4b illustrates the point in the KE time series for the separated IC: the first relative max-

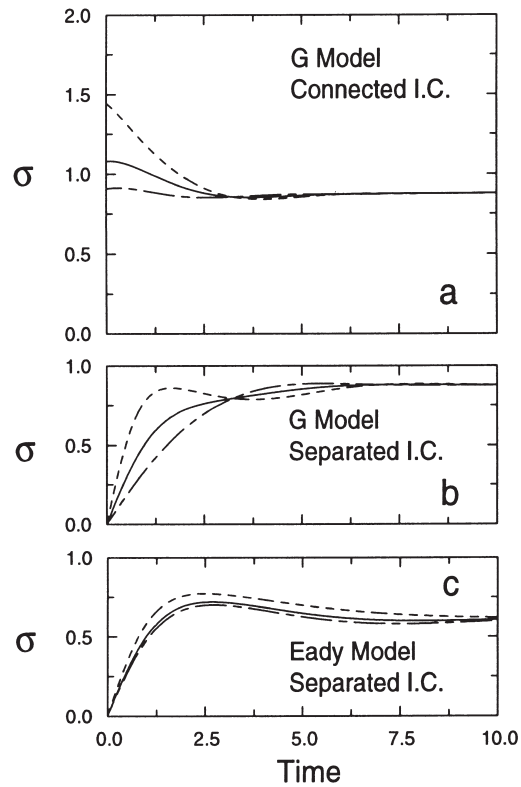


Fig. 4. Growth rates of quasi-geostrophic energy and its components versus nondimensional time. Total energy, E (solid line) with components kinetic energy, KE (short dashed line) and available potential energy, APE (dot-dashed line). Results shown are the G model using (a) connected and (b) separated IC and (c) the Eady model using the separated IC.

imum (near $t = 1.3$) is clearly NG-related while the curve after $t = 4$ looks like an emerging normal mode. As with the connected case, there is more NG for the KE than for the APE . Consulting Table 2, one sees that the initial ratio of KE over APE is much less for both ICs (by a factor of ~ 2) than the normal mode value. This result seems similar to the potential enstrophy result that NG is stronger the more a component in the IC is less than the asymptotic value. One can see this effect by reconsidering modified ICs introduced in the potential enstrophy discussion.

When the separated IC is modified to have larger BPV at the bottom (the “linear” IC) there is slightly more APE as well. Since APE is the largest component (Table 2) this means that the

corresponding KE/APE ratio is slightly farther from its asymptotic value. The peak growth rate of KE during the first 4 units of time is slightly greater for this case, as is the E growth rate during that time. Even so, the EG ratio remains below 1. The “vertical” IC has neither vertical tilt nor vertical amplitude change in the troposphere, so the initial APE is nearly zero. The growth rate of KE shows no evidence for NG while the EG ratio for APE is very large and stays above 2.0 for the first unit of time and above 1 for the first 2.5 units. While APE remains a small component of E during the first unit of time, it is large enough to affect the E growth rate which ultimately exceeds the normal mode value ($EG = 1.06$ at $t = 2.4$).

The results for the Eady model are similar to the G model with two primary exceptions noted before: the asymptotic approach to the normal mode profile is slower and NG is stronger for comparable integral quantities and ICs. Like the G model, the Eady model also has stronger NG in the connected than in the separated IC simulations (Table 1). Total energy and APE both have NG for the separated IC in the Eady model (Fig. 4c), where less is apparent in the corresponding G model simulation (Fig. 4b). The differences between Eady and G model results are again elucidated by introducing one improvement at a time to the Eady model and reconsidering the separated IC. EG ratios for KE and APE are little altered by including compressibility or realistic static stability. The zonal wind profile lowers the EG ratio for KE and for APE by about 15%. The linearly-varying Coriolis parameter lowers the EG ratios of KE and APE by 10–15%. Hence, all the improvements upon the Eady model lower the apparent NG for energy components.

4. Conclusions

This study revisits QG baroclinic instability and nonmodal growth (NG) with a focus upon how the components of energy (E) and potential enstrophy (H) evolve over time. Tracking the components elucidates the evolution of the total quantity. The Eady model and the G model are emphasized; the latter uses linearly-variable Coriolis, compressibility, “realistic” static stability and basic state wind. The impacts upon NG are described for these model improvements. Two

initial conditions (IC) are emphasized, one used by several other researchers (the “connected” IC) and the other more similar to observed cyclogenesis precursors (the “separated” IC). These ICs represent broader classes of initial states. The solutions asymptote to the most unstable structure. The “EG ratio” is introduced to provide a simple, but approximate measure of the NG present; it is the ratio of the peak growth rate over the asymptotic value. Ratios of root mean square (RMS) values of the components of H and E prove useful to interpret the evolution of H , E , and their components.

The primary results are as follows.

- H growth is mainly ($\sim 90\%$) by meridional BPV fluxes for these initial conditions and both models. TV flux comprises the remainder.
- Peak growth rate of BPV^2 is much larger when RMS BPV differs markedly from the unstable normal mode value. ICs with small BPV have greater NG in H . However, small adjustments can have large impact on BPV and thus upon the EG ratio for H . Hence, a simple indicator of NG in H may be the amount of BPV present at the bottom relative to other components of H .
- The more the ratio of RMS APE to RMS KE exceeded the normal mode value, the larger was NG in KE and E .
- The G model had significantly less NG than the Eady model for E , KE, APE, RV, L2, and TV. Testing of the improvements upon the Eady model revealed that they all tended to reduce NG of E , KE, and APE. For H and its components, variable Coriolis increased NG (in part by reducing the asymptotic growth rate) while realistic mean flow reduced it (in part by increasing the asymptotic growth rate). RV^2 and KE tended to show less sensitivity to the model improvements than other corresponding components. These results contrast somewhat with the normal mode sensitivity. Adding compressibility and realistic static stability to the Eady model increases the maximum growth rate only slightly, and shifts it to a shorter wavelength (Green 1960).
- The “tilting into the vertical” conceptual model of NG does not always apply. H had large NG even as upstream tilt was developing due to growth by BPV exceeding adjustments between RV and TV.
- The “superposition” conceptual model remained uniformly valid as judged from projecting

the total solution onto the eigenmodes. However, such projections are tedious in practice.

5. Acknowledgments

This work was performed in partial fulfillment of DH's M. S. degree. DH acknowledges helpful

conversations provided through the course of this work with Drs. T. Nathan, J. Tribbia and E. O'Brien. Also, the authors acknowledge the generous support provided by the National Science Foundation through grant ATM-9615316.

REFERENCES

- Bretherton, F. P. 1966. Critical layer instability in baroclinic flows. *Quart. J. Roy. Met. Soc.* **92**, 325–334.
- Charney, J. G. 1947. The dynamics of long waves in a baroclinic westerly current. *J. Meteor.* **4**, 135–162.
- Davies, H. and Bishop, C. 1994. Eady edge waves and rapid development. *J. Atmos. Sci.* **51**, 1930–1946.
- Dong, B. and James, I. 1997. The effect of barotropic shear on baroclinic instability Part II: The initial value problem. *Dyn. Atmos. Oceans* **25**, 169–190.
- Eady, E. T. 1949. Long waves and cyclone waves. *Tellus* **1**, 33–52.
- Farrell, B. 1982. The initial growth of disturbances in a baroclinic flow. *J. Atmos. Sci.* **39**, 1663–1686.
- Farrell, B. 1984. Modal and nonmodal baroclinic waves. *J. Atmos. Sci.* **41**, 668–673.
- Farrell, B. 1985. Transient growth of baroclinic waves. *J. Atmos. Sci.* **42**, 2718–2727.
- Fischer, C. 1998. Linear amplification and error growth in the 2D Eady problem with uniform potential vorticity. *J. Atmos. Sci.* **55**, 3363–3380.
- Green, J. 1960. A problem in baroclinic stability. *Quart. J. Roy. Meteor. Soc.* **86**, 237–251.
- Grotjahn, R. 1980. Linearized tropopause dynamics and cyclone development. *J. Atmos. Sci.* **37**, 2396–2406.
- Grotjahn, R. 1993. *Global atmospheric circulations: observations and theories*. Oxford University Press, NY. 430 pp.
- Grotjahn, R. 1996. Composite trough evolution of selected west pacific extratropical cyclones. *Mon. Wea. Rev.* **124**, 1470–1479.
- Grotjahn, R. and Tribbia, J. 1995. On the mechanism of cyclogenesis as deduced from vertical axis tilts. *Tellus* **47A**, 629–637.
- Grotjahn, R., Chen, M. and Tribbia, J. 1995a. Linear instability with Ekman and interior friction. Part I: Quasigeostrophic eigenanalysis. *J. Atmos. Sci.* **52**, 754–763.
- Grotjahn, R., Pedersen, R. and Tribbia, J. 1995b. Linear instability with Ekman and interior friction. Part II: Initial value analysis. *J. Atmos. Sci.* **52**, 764–777.
- Hakim, G. 2000. Role of nonmodal growth and nonlinearity in cyclogenesis initial-value problems. *J. Atmos. Sci.* **57**, 2951–2967.
- Joly, A. 1995. The stability of steady fronts and the adjoint method: nonmodal frontal waves. *J. Atmos. Sci.* **52**, 3082–3108.
- Lindzen, R. and Tung, K. 1978. Wave overreflection and shear instability. *J. Atmos. Sci.* **35**, 1626–1632.
- O'Brien, E. 1992. Optimal growth rates in the quasigeostrophic initial value problem. *J. Atmos. Sci.* **49**, 1557–1570.
- Rotunno, R. and Fantini, M. 1989. Petterssen's type B cyclogenesis in terms of discrete, neutral Eady modes. *J. Atmos. Sci.* **46**, 3599–3604.
- Rotunno, R. and Bao, J.-W. 1996. A case study of cyclogenesis using a model hierarchy. *Mon. Wea. Rev.* **124**, 1051–1066.
- Simmons, A. and Hoskins, B. 1979. The upstream and downstream development of unstable baroclinic waves. *J. Atmos. Sci.* **36**, 1239–1254.
- U.S. Committee on Extension to the Standard Atmosphere, 1976. *US Standard Atmosphere, 1976*, U.S. Govt. Print. Off. Washington, D.C., 227 pp.